BC ARTICLE



Lanthanide-dependent alcohol dehydrogenases require an essential aspartate residue for metal coordination and enzymatic function

Received for publication, February 25, 2020, and in revised form, April 30, 2020 Published, Papers in Press, May 4, 2020, DOI 10.1074/jbc.RA120.013227

Nathan M. Good^{1,‡}, Matthias Fellner^{2,3,‡}, Kemal Demirer^{1,4}, Jian Hu^{2,5}, Robert P. Hausinger^{1,2}, and N. Cecilia Martinez-Gomez^{1,*}

From the ¹Department of Microbiology and Molecular Genetics, Michigan State University, East Lansing, Michigan, USA, the ²Department of Biochemistry, Michigan State University, East Lansing, Michigan, USA, ³Department of Biochemistry, University of Otago, Dunedin, Otago, New Zealand, ⁴Okemos High School, Okemos, Michigan, USA, and the ⁵Department of Chemistry, Michigan State University, East Lansing, Michigan, USA

Edited by Ruma Banerjee

The lanthanide elements (Ln³⁺), those with atomic numbers 57-63 (excluding promethium, Pm³⁺), form a cofactor complex with pyrroloquinoline quinone (PQQ) in bacterial XoxF methanol dehydrogenases (MDHs) and ExaF ethanol dehydrogenases (EDHs), expanding the range of biological elements and opening novel areas of metabolism and ecology. Other MDHs, known as MxaFIs, are related in sequence and structure to these proteins, yet they instead possess a Ca2+-PQQ cofactor. An important missing piece of the Ln3+ puzzle is defining what features distinguish enzymes that use Ln3+-PQQ cofactors from those that do not. Here, using XoxF1 MDH from the model methylotrophic bacterium Methylorubrum extorquens AM1, we investigated the functional importance of a proposed lanthanide-coordinating aspartate residue. We report two crystal structures of XoxF1, one with and another without PQQ, both with La3+ bound in the active-site region and coordinated by Asp³²⁰. Using constructs to produce either recombinant XoxF1 or its D320A variant, we show that Asp³²⁰ is needed for *in vivo* catalytic function, in vitro activity, and La3+ coordination. XoxF1 and XoxF1 D320A, when produced in the absence of La³⁺, coordinated Ca²⁺ but exhibited little or no catalytic activity. We also generated the parallel substitution in ExaF to produce ExaF D319S and found that this variant loses the capacity for efficient ethanol oxidation with La³⁺. These results provide evidence that a Ln³⁺-coordinating aspartate is essential for the enzymatic functions of XoxF MDHs and ExaF EDHs, supporting the notion that sequences of these enzymes, and the genes that encode them, are markers for Ln³⁺ metabolism.

Pyrroloquinoline quinone (PQQ) is the prosthetic group of a large class of eight-bladed β propeller dehydrogenases that catalyze the oxidation of alcohols and aldose sugars (1–3). Quinoproteins are generally known as periplasmic enzymes from Gram-negative bacteria, many of which are capable of synthesizing PQQ themselves. PQQ is also known to be physiologically important for plants (4) and mammals (including humans) (5), and PQQ-dependent enzymes have been identified in

eukaryotes (6, 7) and archaea (8). Relatively little is known about the functions or activities of these enzymes, yet the emergence of PQQ enzymes in these domains suggests that quinoproteins have been greatly undersampled in nature.

In the "classic" (PQQ-containing) quinoprotein active site, calcium (Ca²⁺) is associated with the prosthetic group to form the cofactor complex (1). Two well-understood representatives of quinoproteins are the prokaryotic Ca²⁺-dependent methanol dehydrogenase (MDH) MxaFI and ethanol dehydrogenase (EDH) ExaA. MxaFI MDH is a critical enzyme for methylotrophy-the ability of microorganisms to derive all carbon and energy needed for survival and growth from reduced compounds lacking carbon-carbon bonds, such as methane and methanol (9-13). A number of recent studies have shown how lanthanide elements (Ln3+) greatly impact methylotrophy. Ln3+ associate with PQQ and function as cofactors of XoxFtype MDHs and ExaF-type EDHs in methylotrophic bacteria (14-17). These enzymes are aptly referred to as Ln³⁺-dependent alcohol dehydrogenases (Ln-ADHs), and their discovery has added Ln³⁺ to the biological table of the elements (15, 16, 18–20). A number of XoxF-type MDHs have been studied from methylotrophic bacteria, with analyses including X-ray crystallography and enzyme kinetics (15, 17, 21–24). ExaF EDH from the model methylotroph Methylorubrum (formerly Methylobacterium (25)) extorquens AM1 is currently the only representative reported from a methylotroph, although genes encoding putative ExaF homologs have been identified in a diverse set of organisms (16, 26, 27). Phylogenetic analyses of XoxF-coding genes indicate that they are widespread in the environment and can be grouped into at least five distinct clades with representatives in Alpha-, Beta-, and Gammaproteobacteria; Verrucomicrobia; and the NC10 phylum bacterium Candidatus "Methylomirabilis oxyfera" (28). Importantly, phylogenetic consideration of potential Ln3+-related genes led to two discoveries: 1) bacteria previously reported to be nonmethylotrophic, such as Bradyrhizobium diazoefficiens USDA110, can indeed grow methylotrophically using XoxF-type MDHs (23), and 2) Ln-ADHs metabolize multicarbon compounds in methylotrophs and nonmethylotrophs, such as Pseudomonas putida KT2440 (16, 29). These relatively recent discoveries underscore the relevance of Ln3+ to microbial diversity and

This article contains supporting information.

[‡] These authors contributed equally to this work.

^{*} For correspondence: N. Cecilia Martinez-Gomez, mart1754@msu.edu.

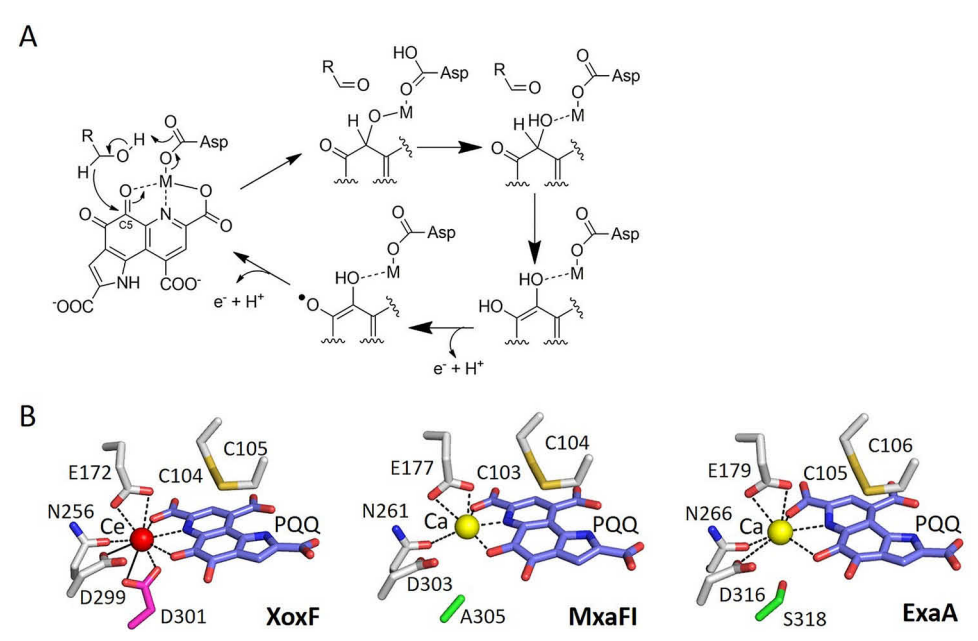


Figure 1. Catalysis of alcohol oxidation by PQQ ADHs. A, catalytic mechanism of alcohol oxidation. The reactive C5 carbonyl of PQQ and Asp required for catalysis are indicated. B, active-site structures of PQQ ADHs: XoxF from M. fumariolicum SoIV (PDB entry 4MAE) (15), MxaFl from M. extorquens AM1 (PDB entry 1W6S) (87), and ExaA from P. aeruginosa (PDB entry 1FLG) (88). The Asp residue depicted in the mechanism (A) corresponds to D299, D303, and D316 in the three structures (B). Slate, PQQ; red sphere, cerium; yellow sphere, calcium; orange, adjacent Cys residues that form a characteristic disulfide; hot pink (XoxF), conserved Asp in Ln ADH; green, Ala (MxaFI) or Ser (ExaA) in the corresponding position in Ca ADH.

emphasize the importance of metal bioavailability in plant, soil, aquatic, and marine ecosystems-complex environments where Ln-utilizing bacteria are major constituents (30-33). Although the use of Ln³⁺ is currently limited to prokaryotic ADHs, the direct association of these metals with PQQ to form a cofactor complex raises the possibility that Ln³⁺ may be linked to all domains of life.

Lighter versions of Ln³⁺, ranging from lanthanum (La³⁺) to europium (Eu³⁺) (atomic numbers 57-63), excluding promethium (Pm3+), have been shown to function with PQQ as essential cofactors in XoxF-type and ExaF-type ADHs. Ln-ADHs can be distinguished from MxaFI-type MDHs and ExaA-type EDHs that bind PQQ and coordinate Ca^{2+} (34, 35). In the heterotetrameric MxaFI MDHs, Ca²⁺ serves as a Lewis acid that polarizes the C5 carbonyl of PQQ, facilitating hydride transfer from the alcohol substrate (Fig. 1A) (36). Because the active site of ExaA-type EDHs is very similar to that of MxaFI, the reaction mechanism is likely analogous (37). Initial reports of Ln-ADHs showing higher catalytic efficiencies compared with Ca-ADHs generated excitement that Ln3+ coordination augmented ADH efficiency as a general phenomenon (15, 16, 28). However, characterization of additional Ln-ADHs included some exhibiting catalytic efficiencies similar to Ca-ADHs (14-17, 21, 22, 28, 29). It is possible that unique physiologies of certain bacteria, such as thermoacidophiles like Methylacidiphilum fumariolicum SolV, require extremely efficient XoxF MDHs for survival (15), but this is likely the exception and not the rule for Ln-ADHs. Functional redundancy may also allow for the adaptation of secondary enzymes for alternative substrates with distinct roles in metabolism, such as formaldehyde oxidation by ExaF (16, 21).

Although Ln-ADHs and Ca-ADHs share many similarities, their clear differences in metal preference raise the question of

what structural features, if any, determine and are potentially diagnostic for metal usage. XoxF-type MDHs are α_2 homodimeric enzymes and distinct from the $\alpha_2\beta_2$ heterodimeric structure of MxaFI-type MDHs (2, 38). One important exception to this generalization is XoxF-type MDH from Candidatus "Methylomirabilis oxyfera," which was purified as a $\alpha_2\beta_2$ heterodimer that included MxaI, the small subunit of MxaFI-type MDHs (24). ExaF-type and ExaA-type EDHs are both α_2 homodimeric enzymes (16, 39). Quaternary structure alone, therefore, cannot be used to differentiate Ln-ADHs and Ca-ADHs. Multiple sequence alignment of type I ADHs, which include both MDHs and EDHs, shows high conservation of catalytically and structurally important amino acids, including Asn, Glu, and Asp residues in the active site (28). Remarkably, one residue is differentially conserved in Ln-ADHs compared with Ca-ADHs (Fig. 1B). Nearly all XoxF and ExaF sequences have an additional Asp residue positioned 2 amino acids downstream from a conserved Asp required for catalytic function (28). This position is occupied by Ala in MxaFI-type MDHs and Ser or Thr in ExaA-type EDHs. The crystal structure of XoxF MDH from M. fumariolicum SolV revealed this additional Asp to coordinate the Ce³⁺, and this residue was proposed to be diagnostic for Ln-ADHs (15, 28). The few XoxF-type MDH crystal structures generally support the role of this residue as being important for Ln³⁺ coordination and function of the enzyme (15-17, 40-42).

M. extorquens AM1 has been a model of study for one-carbon metabolism for decades. This methylotrophic bacterium produces XoxF1 MDH and ExaF EDH that both contain Ln-PQQ cofactors (13, 21, 43-45) and possess the additional Asp residue proposed to be important for Ln³⁺ coordination: Asp³²⁰ (XoxF1) and Asp³¹⁹ (ExaF), respectively. XoxF1 and ExaF have been kinetically characterized with La³⁺, and XoxF1



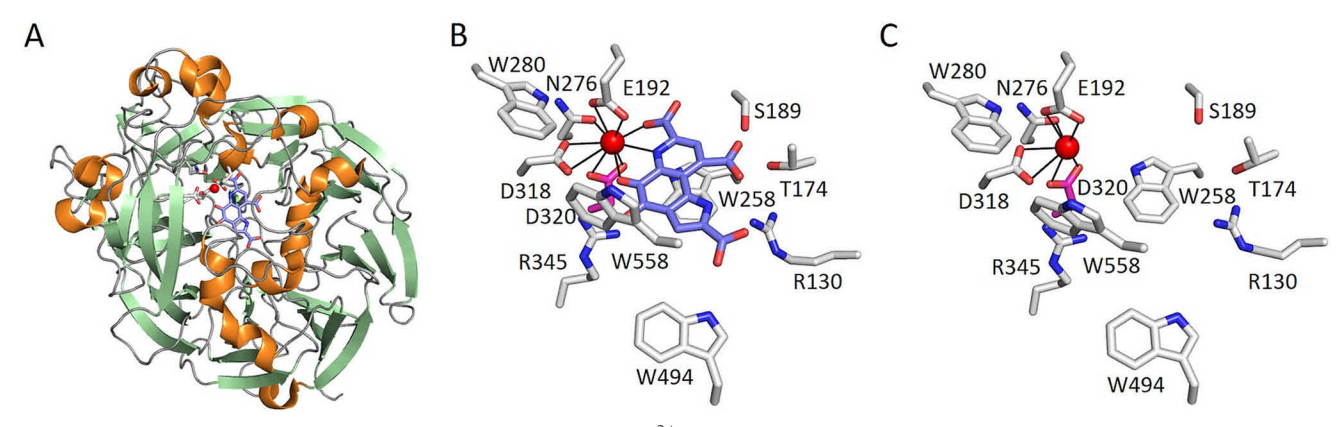


Figure 2. *M. extorquens* AM1 XoxF1 crystal structures. *A*, overall fold (La³⁺-PQQ model shown, PDB entry 6OC6) with *β*-sheets in *pale green*, α -helices in *orange*, and coils in *gray*. The active site is illustrated with La³⁺ in *red*, chelating residues in *white*; PQQ in *slate*, oxygen atoms in *red*, and nitrogen atoms in *blue*. *B*, XoxF1-La³⁺-PQQ active site with metal-coordinating residues *labeled*; Ln-coordinating Asp in *hot pink*. *C*, XoxF1-La³⁺ active-site region. La³⁺ and residues shown are the same as depicted in *B*.

with neodymium as well (16, 21). M. extorquens AM1 can produce a second XoxF MDH that is \sim 90% identical to XoxF1 (46). The protein has been named XoxF2, and its function in the WT strain is still not well-understood. XoxF2 is capable of supporting methanol growth with Ln3+ when XoxF1 cannot be produced, although it seems to be a secondary enzyme (43). M. extorquens AM1 also produces the Ca²⁺-dependent MxaFI MDH. Expression of the mxa operon, encoding MxaFI and accessory/Ca²⁺-insertion proteins, is differentially regulated from the xox1 gene cluster by the "Ln switch" that is sensitive to the presence of nanomolar Ln³⁺ (43, 47, 48). When Ln³⁺ are absent from the growth medium (or at sub-nanomolar concentrations), xox1 expression is down-regulated and mxa expression is up-regulated. If Ln3+ are present at nanomolar or greater concentrations, mxa expression is down-regulated and xox1 is highly expressed (21). The presence of the Ln switch in M. extorquens AM1 and the capacity to produce Ca-MDH and Ln-ADH make it an excellent model for the study of Ln biology.

Of the few reported Ln-ADHs, all have the hypothetical "Ln-coordinating Asp" including XoxF1 and ExaF from M. extorquens AM1. Although theoretical studies support the importance of this residue for the function of Ln-ADH, no empirical study, until now, has shown that this residue is required for Ln3+ coordination and catalytic function of these enzymes. We report the structure of XoxF1 from *M. extorquens* AM1 as a representative Type V XoxF MDH structure. The protein crystallized as a homodimer with one La³⁺ and one PQQ per subunit. We report an additional structure with only La³⁺ coordinated; this is the first structure of an MDH without PQQ bound to our knowledge. In both structures, Asp³²⁰ contributes to La³⁺ coordination. Using site-directed mutagenesis, we constructed an Ala³²⁰ substitution variant of XoxF1 (D320A) from M. extorquens AM1 and show that the mutant cells were incapable of growth with methanol and La³⁺. MDH activity was only detectable for XoxF1, and not for XoxF1 320A, when purified from cultures grown with La³⁺. When purified from cultures lacking La³⁺, XoxF1 and XoxF1 D320A exhibited little to no activity with methanol. Further, we show that production of catalytically inactive XoxF1 from plasmid constructs was sufficient to allow for MxaFI-dependent growth on methanol in a $\Delta xoxF1$ $\Delta xoxF2$ mutant. Finally, we report that an

ExaF D319S variant (the parallel substitution to XoxF1 D320A) was inactive with ethanol *in vivo*, providing evidence that the Ln-coordinating Asp is also necessary for catalytic function of ExaF-type EDHs. Overall, this study provides empirical evidence in support of the Ln-coordinating Asp being necessary for Ln-ADH catalytic function and supports its potential use as a marker to identify new Ln-ADHs.

Results

Crystal structures of XoxF1 with La³⁺

The number of Ln-ADH crystal structures available is limited, and more representatives are needed to better understand structural similarities and differences among Ln- and Ca-ADHs. Currently, only three structures are available for study: XoxF from M. fumariolicum SolV with Ce³⁺ or Eu³⁺ (PDB entry 4MAE (15) or 6FKW (49)) and XoxF from Methylomicrobium buryatense 5GB1C with La3+ (PDB entry 6DAM (17)). The enzyme from M. fumariolicum SolV falls within the type II clade of XoxF MDH, and that from M. buryatense is a type V enzyme. Both of these organisms are methanotrophs (capable of oxidizing methane to methanol), whereas M. extorquens AM1 cannot oxidize methane. M. extorquens AM1 has a type V enzyme, XoxF1, which was the first Ln-ADH described in the scientific literature (14). Using immobilized metal affinity chromatography (IMAC), we purified recombinant XoxF1 fused to a hexahistidine tag from cultures grown in minimal methanol medium with 20 μM LaCl₃. After tag cleavage and concentration to 2.5 mg/ml, the protein was crystallized (see "Experimental procedures"). Two XoxF1 structures were resolved: one in complex with La3+-PQQ, and a second with only La³⁺ bound (Fig. 2). The overall structures, both showing two protein chains in each asymmetric unit, are nearly identical with a $C\alpha$ alignment resulting in a root mean square deviation (RMSD) of ~0.3 Å comparing chains across and within the two structures (Table S1). All chains are fully built from residue Asn²² to the penultimate C-terminal residue, Asn⁶⁰⁰. The missing N-terminal residues were previously identified as a likely signal peptide for translocation from the cytoplasm to the periplasm (28). The overall fold matches other MDHs with the typical eight-bladed β -sheet propeller surrounding the active site (Fig. 2A) (1, 2, 17, 28, 38, 50–53). Comparison with the most closely related methanol dehydrogenases with available structures shows minor deviations in surface-exposed loops: M. buryatense 5G XoxF (PDB entry 6DAM (17)) had \sim 0.5-Å C α RMSD with 67% sequence identity, and M. fumariolicum SolV XoxF (PDB entry 4MAE (15) or 6FKW (49)) had \sim 0.7-Å C α RMSD with 55% sequence identity (Fig. S1A).

The active-site regions of the XoxF1-La³⁺-PQQ (Fig. 2B and Fig. S2A) and XoxF1-La³⁺ (Fig. 2C and Fig. S2B) show a high degree of similarity. La³⁺ is coordinated the same way in both structures using Glu¹⁹² (bidentate), Asn²⁷⁶ (monodentate via oxygen), Asp³¹⁸ (monodentate), and Asp³²⁰ (bidentate). PQQ introduces three additional coordination atoms (two oxygen and one nitrogen) for the first structure. Residues surrounding PQQ show similar side-chain rotamers in both XoxF1-La³⁺-PQQ and XoxF1-La3+ structures. In the La3+-only bound structure, chain A is 100% occupied by the metal, and one of the PQQ coordination sites is occupied by a small molecule that we interpreted conservatively as a water. Chain B appears to be more disordered in the active site region, and the La³⁺ atoms refined to 59% occupancy, indicating that 41% of the structure is in the metal-free state. This situation led to greater mobility of Trp²⁸⁰, Asp³¹⁸, and Arg³⁴⁵ side chains, likely indicating alternative conformations (Fig. S2, B-D). In addition, Trp^{258} possibly shows a second conformation pointing toward La³⁺ and partially occupying its space in the metal-free portion of the protein; however, at an overall resolution of 2.8 Å, the minor alternate state of the protein could not be modeled with confidence. Given the apparent flexibility of these four residues, they may play a role in metal binding and metal release even though they do not directly coordinate the La³⁺. Alternatively, these residues could passively fill the cavity when ${\rm La}^{3+}$ is not present. Notably, the conformation of Asp³²⁰ did not change with decreased metal occupancy, indicating likely inflexibility at this position (Fig. S2, B and C). We speculate that PQQ was also present in the XoxF1-La3+ sample during its purification but that the crystal conditions (with 10% propanol) resulted in release of the organic portion of the cofactor in both chains and partial loss of La³⁺ in chain B. When we regrew these crystals, substituting propanol with 10% methanol, we again obtained the XoxF1-La³⁺ structure lacking PQQ (data not shown). The implications of these observations are that XoxF1 coordinates La³⁺ even though PQQ is no longer part of the cofactor complex.

To compare with existing structures, we compiled a list of related MDH structures by cross-referencing entries of Pfam family PQQ_2 (PF13360) (54) having 25% sequence identities to M. extorquens XoxF1 in the Protein Data Bank (55), as well as three-dimensional structure hits better than 2.1-Å RMSD in DALI (56). Nineteen structures were examined after excluding six structures that shared the overall fold, but not the general active site environment, and we found that all proteins had both the metal and PQQ bound in the active site. The XoxF1-La³⁺ structure reported here is currently the only PQQ-free structure of this family, and notably the "organic cofactor-less" enzyme maintained the homodimer quaternary structure. From 11 unique proteins, the XoxF1 La³⁺-PQQ active site

environment is very similar to the two most closely related Ln-ADH (La³⁺-PQQ (6DAM), Ce³⁺-PQQ (4MAE), and Eu³⁺-PQQ (6FKW)). In all cases, the same protein side chain and PQQ metal chelation is observed, suggesting that light Ln³⁺ share the same coordination in this state (Fig. S1B), as predicted by DFT calculations (40, 57). The nine remaining proteins have a Ca²⁺ atom (with one Mg²⁺ exception) bound in their structures. The main difference to XoxF1 from M. extorquens AM1 is seen in the position corresponding to Asp³²⁰, where the Ca²⁺-binding proteins have either an Ala, Ser, or Thr residue (Fig. S1C).

Substitution of Asp³²⁰ with Ala abolishes XoxF1 function with La³⁺ in vivo

To test the necessity of the additional aspartate residue for Ln³⁺-dependent function of XoxF1 from *M. extorquens* AM1, we designed expression constructs to produce the WT protein and an $Asp^{320} \rightarrow Ala$ substitution variant, subsequently referred to as XoxF1 D320A. Substitution of Asp³²⁰ with Ala mimics the corresponding residue in MxaFI, the large subunit of MxaFI Ca-MDH in this microorganism. We chose to express WT and variant MDH-encoding genes via the constitutive M_{tac} promoter to bypass the complex regulatory network involved in mxa and xox1 gene expression. We anticipated that expression from M_{tac} would be reduced compared with native P_{mxa} and P_{xox1} expression levels, and the corresponding enzyme activities would be lower in vivo. As such, we tested for construct functionality in the $\Delta xoxF1$ $\Delta xoxF2$ double mutant strain (Table 1) that cannot produce XoxF MDH but retains a genomic copy of exaF. ExaF exhibits relatively low MDH activity with Ln^{3+} , allowing the $\Delta xoxF1$ $\Delta xoxF2$ strain to slowly grow (~15% of the rate of WT cells) using methanol as the substrate (Fig. 3, A and C), but only if Ln^{3+} are added to the growth medium. We anticipated increased growth if functional MDH was produced from our constructs. When XoxF1 was produced in the $\Delta xoxF1$ $\Delta xoxF2$ background and cells were grown with methanol and La3+, the culture growth rate increased by 25% and the culture growth yield increased by 67% compared with the empty plasmid control strain, $\Delta xoxF1 \Delta xoxF2$ /empty (p < 0.001 by one-way analysis of variance (ANOVA)) (Fig. 3, A and C). These results indicated the plasmid produced functional XoxF1. The strain producing XoxF1 D320A, on the other hand, grew at the same rate as the control strain and reached a similar final culture yield, suggesting that XoxF1 D320A was not functional in this condition.

XoxF1 and XoxF1 D320A allow for equivalent growth on methanol with Ca2+

XoxF is required for expression of *mxa* and, by implication, production of MxaFI Ca-MDH (58). The $\Delta xoxF1$ $\Delta xoxF2$ double mutant strain retains the *mxa* operon encoding MxaFI, but it cannot grow on methanol without the addition of Ln³⁺ because it cannot produce XoxF protein to up-regulate mxa expression (43, 58). We observed growth of the $\Delta xoxF1 \Delta xoxF2$ strain on methanol without adding Ln3+ when we complemented the cells with the XoxF1 construct (Fig. 3B). These results provided additional confirmation of expression by the



Table 1Bacterial strains and plasmids used in this study

Strain or plasmid	Description	Reference/Source	
Strains			
Escherichia coli			
DH5 α	Electrocompetent cloning strain	Invitrogen	
S17-1	Conjugating donor strain	Ref. 83	
Methylorubrum extorquens			
AM1	WT; rifamycin-resistant derivative	Ref. 84	
$\Delta mxaF$	Deletion mutant	Ref. 85	
$\Delta xoxF1 \ \Delta xoxF2$	Double deletion mutant	Ref. 58	
ADH-4	$\Delta mxaF \Delta xoxF1 \Delta xoxF2 \Delta exaF$ quadruple deletion mutant	Ref. 21	
Plasmids			
pRK2013	Helper plasmid, IncP <i>tra</i> functions, K _m ^r	Ref. 86	
pHC61	K_{m}^{r} , M_{tac} -empty	Ref. 70	
pNG284	K_{m}^{r} , P_{vor} -xoxF1, TEV cleavage site, hexahistidine tag	Ref. 21	
pNG286	K_m^r , P_{rev} -exaF, TEV cleavage site, hexahistidine tag	This study	
pNG265	K_{m}^{r} , P_{xoxI} -exaF, Xa cleavage site, hexahistidine tag	Ref. 16	
pNG311	K_m^r , M_{tac} -empty, TEV cleavage site, hexahistidine tag	This study	
pNG308	K_m^r , M_{tac} -xoxF1, TEV cleavage site, hexahistidine tag	This study	
pNG309	$K_{\rm m}^{\rm r}$, M_{tac} -xoxF1 D320A, TEV cleavage site, hexahistidine tag	This study	
pNG305	K_{m}^{r} , M_{tac} -exaF, TEV cleavage site, hexahistidine tag	This study	
pNG307	K_m^{mr} , M_{tac} -exaF D319S, TEV cleavage site, hexahistidine tag	This study	

constructs. Double mutant cells carrying the construct producing XoxF1 attained a growth rate and yield similar to the WT strain (Fig. 3*C*). This result suggested that XoxF1 produced from our construct was enough to up-regulate production of MxaFI MDH for methanol growth with Ca²⁺. Although we could not yet rule out the possibility that XoxF1 produced from our construct was using Ca²⁺ in place of Ln³⁺ for catalysis, previous work had shown that recombinant XoxF1 purified in the absence of Ln³⁺ exhibited only poor activity and was insufficient to support growth with methanol as the sole MDH (59). Therefore, we did not consider XoxF1 to be a significant contributor to MDH activity without Ln³⁺. Even so, that same study did not establish whether XoxF1 bound Ca²⁺, leaving that question unanswered.

In the current study, we also tested the $\Delta xoxF1$ $\Delta xoxF2$ mutant producing XoxF1 D320A for methanol growth without the addition of Ln³+ (Fig. 3B). The growth rate was identical to that of the WT/empty strain, indicating that the enzyme variant was able to execute its regulatory role for production of MxaFI Ca-MDH. The final growth yield of the culture, on the other hand, was reduced by 58% (p < 0.001 by one-way ANOVA) (Fig. 3D). To assess whether catalytic function of the XoxF1 D320A variant was responsible for the growth defect, we conducted MDH activity assays with purified enzymes.

Asp^{320} is required for catalytic function of XoxF1 MDH with Ln^{3+}

Growth augmentation was observed for the $\Delta xoxF1$ $\Delta xoxF2/$ XoxF1 strain when provided with La³⁺, indicating that XoxF1 was catalytically active. In contrast, analogous cells producing XoxF1 D320A showed no increase in their growth upon La³⁺ addition, indicating that the variant was inactive. To confirm this conclusion, 1.5-liter cultures of $\Delta xoxF1$ $\Delta xoxF2$ producing either enzyme were grown in minimal methanol medium with La³⁺, and the XoxF1 and XoxF1 D320A enzymes were purified from cell-free extracts by IMAC. SDS-PAGE demonstrated the successful enrichment and relative purity of both enzymes (Fig. 4A). XoxF1 and XoxF1 D320A were desalted, and MDH activity was measured via the phenazine

methosulfate (PMS)-mediated reduction of 2,6-dichlorophenol indophenol (DCPIP) (43, 60). XoxF1 was found to be active, although the specific activity with saturating substrate ($V_{\rm max}$) was only ~50% of what we had observed in an earlier study (Fig. 4C) (21). This result suggested that the XoxF1 used here was not fully loaded with La³+. An equal amount or up to 6-fold greater level of XoxF1 D320A lacked detectable activity, suggesting that the enzyme did not bind La³+ (Fig. 4C). We previously reported that XoxF1 was not reconstituted by La³+ (21). Nonetheless, we tested whether the addition of equimolar LaCl₃ affected the assay of XoxF-D320A (in case the variant enzyme could weakly bind La³+, or if the metal was lost during purification and/or desalting); however, no MDH activity was observed.

Substitution of Asp³²⁰ with Ala in XoxF1 approximates the coordination environment of the MxaFI active site. We wondered, therefore, if this amino acid substitution could effectively convert XoxF1 from a Ln³⁺-dependent MDH to a Ca^{2+} -dependent enzyme. Phenotypic studies of $\Delta xoxF1$ $\Delta xoxF2/XoxF1$ D320A cells showed that this strain was able to grow on methanol without the addition of Ln3+, suggesting that the variant could be active with Ca²⁺. To investigate this possibility further, the $\Delta xoxF1$ $\Delta xoxF2$ double mutant producing either XoxF1 or XoxF1 D320A was grown in minimal methanol medium without the addition of exogenous La³⁺. The IMAC-purified XoxF1 and XoxF1 D320A samples (Fig. 4B) were examined for their MDH activities. XoxF1 exhibited detectable activity, as also observed in a previous report (note that that the variance among our measurements was relatively high, but all measured activities were low) (59). The poor activity observed for XoxF1 purified without La³⁺ raises the question of whether the enzyme can coordinate Ca²⁺ when the Ln switch is not induced. In contrast, the XoxF1 D320A variant enzyme purified from the same culture condition exhibited no detectable MDH activity. The combined assay results for the XoxF1 D320A variant suggest that the Asp to Ala substitution rendered the enzyme inactive and show that it was not enough to convert XoxF1 into an efficient Ca²⁺-dependent MDH.

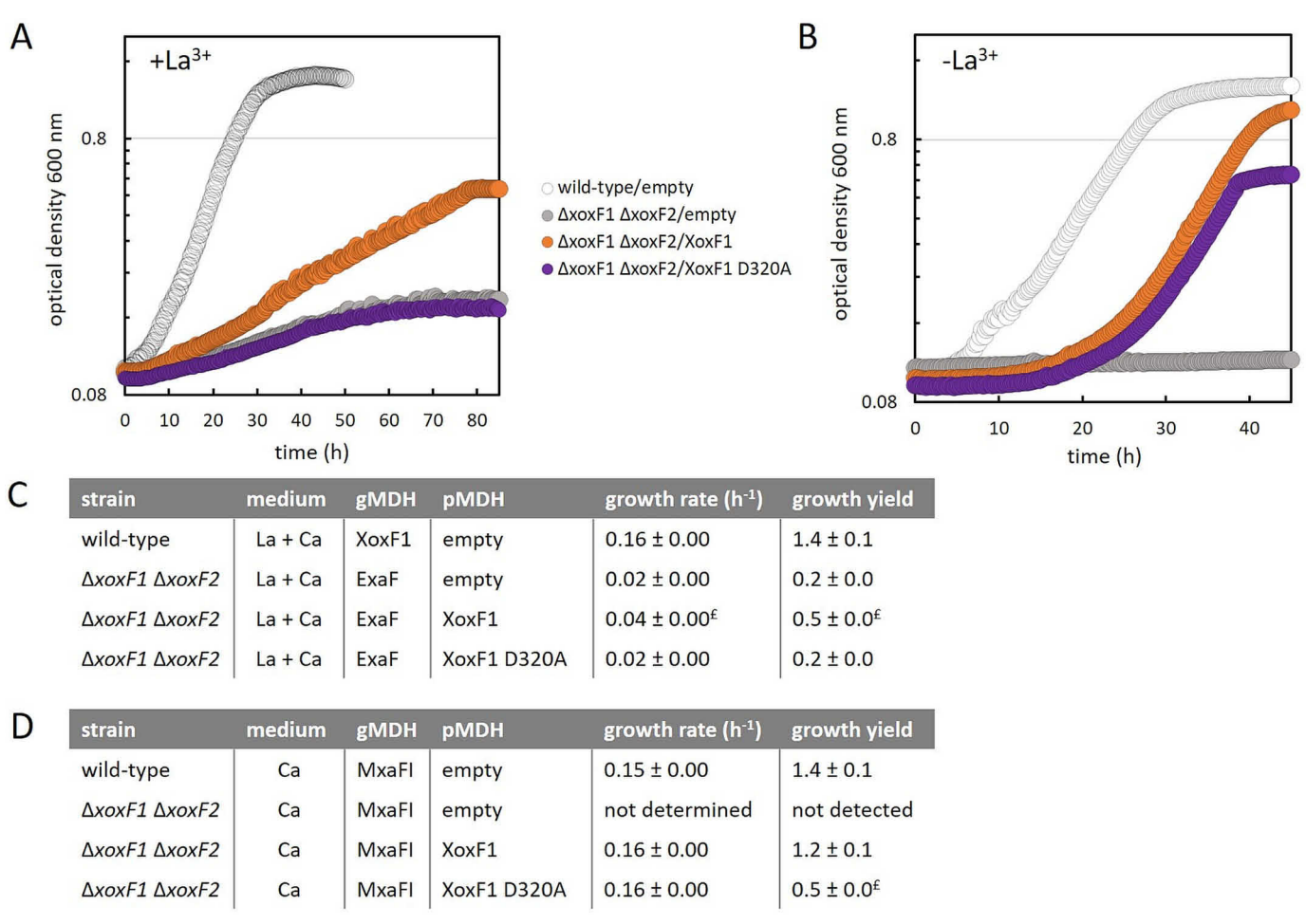


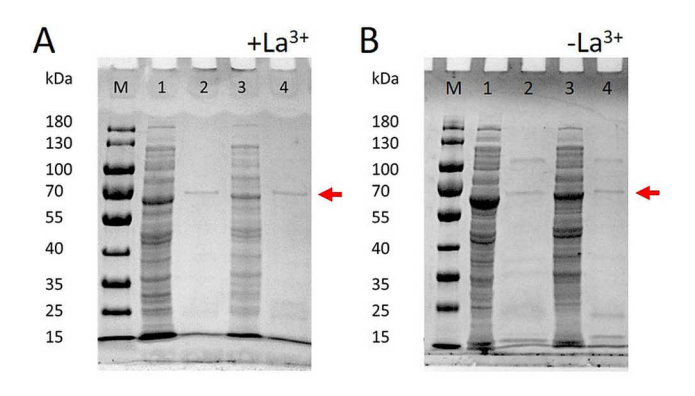
Figure 3. Expression of xoxF1 and xoxF1 D320A impacts growth on methanol in a metal-dependent manner. Growth analysis of the $\Delta xoxF1$ $\Delta xoxF2$ MDH mutant strain carrying expression plasmids producing XoxF1 or XoxF1 D320A in methanol medium with the addition of La³⁺ (A) or without the addition of La³⁺ (B). White, WT cells carrying the empty plasmid; gray, $\Delta xoxF1$ $\Delta xoxF2$ mutant carrying the empty plasmid; orange, $\Delta xoxF1$ $\Delta xoxF2$ carrying the plasmid to produce XoxF1; purple, $\Delta xoxF1$ $\Delta xoxF2$ carrying the plasmid to produce XoxF1 D320A. Growth curves are representative of a minimum of 12 biological replicates from at least two independent experiments. Replicate data points were within 5%. C, growth rates and growth yields for the WT and $\Delta xoxF1$ $\Delta xoxF2$ mutant strains from A. D, growth rates and growth yields for the WT and $\Delta xoxF1$ $\Delta xoxF2$ mutant strains with expression plasmids from B. In both tables C and D, gMDH refers to the genome-encoded ADH catalyzing methanol oxidation; pMDH refers to the plasmid-encoded MDH; empty, no MDH is encoded in the plasmid. Errors shown for growth rates and growth yields are RMSE and S.D., respectively, for a minimum of 12 biological replicates from at least two independent experiments. £, a change of statistical significance at p < 0.001 by one-way ANOVA from the $\Delta xoxF1$ $\Delta xoxF2$ strain carrying the empty plasmid.

Metal content of XoxF1 and XoxF1 D320A

Purified XoxF1 and XoxF1 D320A produced in cultures grown with and without La³⁺ were analyzed for metal content using inductively coupled plasma (ICP)-MS for La³⁺ or ICPoptical emission spectroscopy (OES) for Ca2+ quantification (Fig. 4C). XoxF1 purified from cells grown in medium with La³⁺ was 39% loaded with La³⁺, corresponding with the MDHspecific activity observed in this study. The partial metal loading observed in this study correlates with our previous work, where we observed a $\sim\!$ 2-fold higher $V_{\rm max}$ for XoxF1 when the enzyme was completely loaded with metal (21). In contrast to the WT enzyme, XoxF1 D320A purified from the same growth medium had only trace amounts of La³⁺ (Fig. 4C), corroborating the importance of Asp³²⁰ to Ln³⁺ binding by this protein. Both the WT and variant enzymes purified from cells grown without added La³⁺ contained trace amounts of La³⁺ likely from glass or reagent contamination, even though all glassware was acid-washed and plastic tubes and bottles were used when possible.

Although XoxF1 is Ln3+-dependent and expression of its gene is tightly regulated by the Ln switch, the reported low MDH activity for XoxF1 purified from culture without added Ln^{3+} suggested that it may have partial function with Ca^{2+} (59). We detected similarly low MDH activity for XoxF1 in this study, and ICP-OES analysis showed the enzyme was completely loaded with Ca2+ (>97%) (Fig. 4C). When La3+ was added to the culture medium, however, Ca²⁺ was not detectable in XoxF1, indicating a strong loading preference for the former metal seemingly to the exclusion of the latter for the WT enzyme. The XoxF1 D320A variant did not exhibit the same metal discrimination; it was loaded with Ca2+ regardless of whether or not La³⁺ was included in the growth medium. Although the D320A substitution does not negatively impact Ca2+ coordination, the enzyme is inactive. These results suggest that the single amino acid substitution remodels the activesite environment enough to disrupt catalysis of methanol oxidation.





C

enzyme	medium	Ca	La	U · mg⁻¹
XoxF1	La + Ca	≤ 0.01	0.4 ± 0.1	2.9 ± 0.1
XoxF1 D320A	La + Ca	1.2 ± 0.6	≤ 0.01	undetectable
XoxF1	Ca	1.0 ± 0.1	≤ 0.01	0.05 ± 0.03
XoxF1 D320A	Ca	0.3 ± 0.0	≤ 0.01	undetectable

Figure 4. XoxF1 D320A is inactive and does not coordinate La. XoxF1 and XoxF1 D320A from cultures of the $\Delta xoxF1 \Delta xoxF2$ mutant carrying an expression plasmid to produce the desired protein and grown in methanol minimal medium with La³+ (A) or without the addition of La³+ (B), thus providing four protein samples. Protein fractions were analyzed by SDS-PAGE for XoxF1 and XoxF1 D320A (predicted M_r of 63 kDa, indicated by a red arrow (21)). M_r protein standard marker; 1, cell-free extracts containing XoxF1; 2, 4 μ g of XoxF1; 3, cell-free extracts containing XoxF1 D320A; 4, 3 μ g of XoxF1 D320A. C_r MDH-specific activity measurements and metal content for the four purified proteins shown in lanes 2 and 4 from A and B. MDH assays were conducted using saturating methanol substrate, with 1 unit of activity defined as 1 μ mol of DCPIP reduced per min and 4 μ g of XoxF1 or 3–18 μ g of XoxF1 D320A for proteins produced with La³+; 4 μ g of XoxF1 or 10–100 μ g of XoxF1 D320A for proteins produced without La³+. Values are the average of six replicates from two independent experiments with S.D. shown. undetectable, no DCPIP reduction was observed. Metal content values are reported as moles of metal per mole subunit of enzyme.

Ln-coordinating Asp is required for efficient ExaF EDH function

To date, all Ln-ADHs fall within the confines of XoxF-type MDHs and ExaF-type EDHs. In this study, we have provided structural, in vivo, and purified enzyme biochemical studies showing that the Ln-coordinating Asp is required for XoxF1 MDH function with La³⁺. To address the question of necessity of this residue in ExaF-type EDHs, we generated expression constructs to produce WT ExaF and its D319S variant. ExaF D319S parallels XoxF1 D320A, where substitution of Asp by Ser at position 319 approximates the active site of ExaA from *P. aeruginosa* (Figs. 1B and 5A), the Ca^{2+} -dependent EDH that is most similar to WT ExaF with an available crystal structure (35, 61–63). Expression constructs were transformed into the ADH-4 mutant strain of *M. extorquens* AM1, which has clean deletions of the four known ADH-encoding genes that allow for growth with methanol or ethanol: mxaF, xoxF1, xoxF2, and exaF. Previously, we reported that the ADH-4 mutant strain was unable to grow in culture tubes with ethanol as the substrate. Using 48-well microplates in this study, however, we observed early poor growth with ethanol in the presence or absence of La³⁺. Because ExaF exhibits high catalytic efficiency using ethanol as the substrate (16), we anticipated that expression of its gene from the M_{tac} promoter would allow for cell growth if the enzyme produced was functional. The ADH-4

mutant strains producing ExaF or ExaF D319S were tested for growth in minimal ethanol medium with and without the addition of La³⁺ (Fig. 5B). The construct producing ExaF complemented the ADH-4 mutant strain when using La³⁺-containing growth medium, with a culture growth rate and yield that were ~41 and ~80% of the WT strain harboring the empty plasmid (Fig. 5C). The reduction in growth yield may have been due to ethanol evaporation from the growth medium as the cultures required an additional 15 h to reach maximal culture density in this condition. Without the addition of La³⁺, ADH-4/ExaF grew marginally better than the ADH-4/empty control strain. The growth rate increased ~3-fold, but the culture did not attain even a 2-fold increase from the initial low density. Combined, these results showed that ExaF did not oxidize ethanol efficiently in this condition, as expected (Fig. 5D). In comparison, ADH-4/ExaF D319S grew similarly with and without the addition of La³⁺, exhibiting marginally increased growth relative to the ADH-4/empty control strain (Fig. 5, B and D). As observed for ADH-4/ExaF without the addition of La³⁺, cultures did not achieve even a 2-fold increase from the starting density, indicating that the enzyme variant was inefficient for ethanol oxidation regardless of metal availability. Importantly, the growth rate and yield of ADH-4/ExaF with the addition of La³⁺ were significantly greater than that of the ADH-4/empty and ADH-4/ExaF D319S strains showing successful complementation (one-way ANOVA, p < 0.001). These results indicate that Asp³¹⁹ is required for efficient ExaF function with Ln³⁺ and likely is important for Ln³⁺ coordination.

Discussion

XoxF-type MDHs are members of type I eight-bladed β propeller quinoproteins (PQQ-containing). MxaFI-type MDHs and ExaF-type EDHs/ADHs fall within the same type I classification (3, 28, 64). Phylogenetic analyses have identified at least five major clades for XoxF-type MDHs and nine additional clades encompassing ExaF-type EDHs/ADHs (18, 28). However, the Ln ADHs available for study are relatively few, and structural data are limited. Here we report two structures of XoxF1 from M. extorquens AM1 (a type V XoxF MDH), one showing coordination of the La³⁺-PQQ cofactor complex and the other with only the La³⁺ atom bound. Both structures confirm coordination of La³⁺ by Asp³²⁰, as has been observed for the corresponding residue in the three previously reported XoxF MDH structures (15, 17, 49), denoting the importance of this residue for Ln3+ coordination and function. Comparative analysis of fully metallated subunits of XoxF1-La3+-PQQ and XoxF1-La³⁺ with the chain B of XoxF1-La³⁺ (61% occupied by ${\rm La^{3+}}$) indicated that ${\rm Asp^{320}}$ is immobile compared with the relatively flexible ${\rm Trp^{258}, Trp^{280}, Asp^{318}}$, and ${\rm Arg^{345}}$ side chains. Asp^{320} may therefore be a key residue for recruiting Ln^{3+} to the active site of XoxF1. In addition, XoxF1-La³⁺ is the first quinoprotein structure reported without PQQ and shows that the organic cofactor is not essential for metal binding even though it provides three coordinating atoms. Incomplete occupancy of La³⁺ in chain B of this structure shows that whereas PQQ likely plays a stabilizing role in Ln³⁺ coordination, it appears to be a minor one. These results imply the Ln3+ may be loaded independently of PQQ when the Ln³⁺-PQQ complex is assembled.



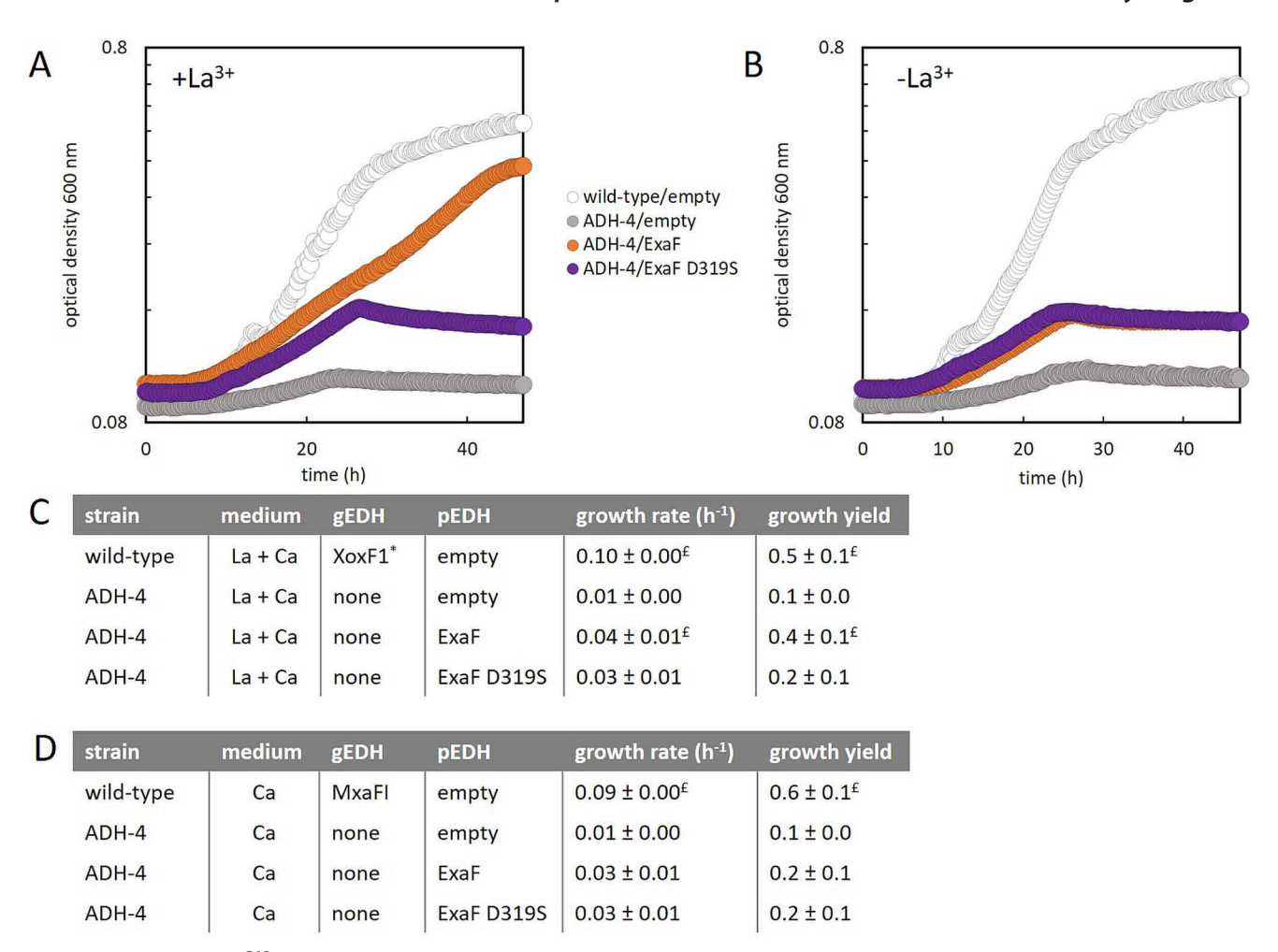


Figure 5. Substitution of Asp³¹⁹ in ExaF EDH with Ser results in loss of function. Growth analysis of the ADH-4 mutant strain carrying expression plasmids producing ExaF or ExaF D319S in ethanol medium with the addition of La³⁺ (A) or without the addition of La³⁺ (B). White, the WT cells carrying the empty plasmid; orange, the ADH-4 mutant carrying the plasmid producing ExaF; gray, the ADH-4 mutant carrying ExaF D319S; purple, the ADH-4 mutant carrying the empty plasmid. Growth curves are representative of a minimum of 18 biological replicates from four independent experiments. Replicate data points were within 5%. C, growth rates and growth yields for strains included in A. D, growth rates and growth yields for strains included in B. In both tables, gEDH refers to the genome-encoded enzyme catalyzing ethanol oxidation; none, the primary oxidation enzyme is unknown. *, proposed active EDH. pEDH, plasmid-encoded EDH; empty, the plasmid does not encode an EDH enzyme. Errors shown for growth rates and growth yields are RMSE and S.D., respectively, for a minimum of 18 biological replicates from four independent experiments. £, a change of statistical significance at p < 0.001 by one-way ANOVA from the ADH-4 strain carrying the empty plasmid and ADH-4 strain expressing exaF D319S.

Additional genetic, biochemical, and structural studies are needed to gain a fuller understanding of the metal-PQQ cofactor assembly, including determination of whether the process is similar for Ca-ADH. Furthermore, dissociation of PQQ from the active enzyme to yield XoxF1-La³⁺ did not disrupt the dimeric structure of the enzyme, as speculated by Featherston et al. (65), showing that PQQ is not essential for maintaining dimeric interface contacts. It remains to be seen whether PQQ is essential for maintaining dimeric and/or tetrameric contacts in MxaFI MDH, ExaA EDH, and other PQQ ADHs.

In this study, we show that substitution of the proposed "Lncoordinating Asp" by Ala renders the XoxF1 D320A variant unable to coordinate La³⁺, resulting in the loss of its MDH function. The parallel substitution yielding ExaF D319S results in loss of its in vivo function as well. Together, these results provide empirical evidence showing the necessity of the additional Asp residue in both XoxF1-type MDHs and ExaF-type EDHs, and they substantiate the Ln-coordinating Asp hypothesis for determining the metal coordination and enzyme function. The identification of putative Ln ADHs by sequence alone has relied on the validity of the Ln-coordinating Asp hypothesis, which we have now corroborated with biochemical and phenotypic evidence. As a result, enzymes that have been marked as putative Ln ADHs can be investigated for Ln utilization with a high degree of confidence, and newly discovered sequences and novel enzymes can be interrogated for the hallmark residue.

Intriguingly, the metal contents of XoxF1 and its D320A variant show that Asp³²⁰ is needed for La³⁺, but not Ca²⁺, binding in vivo. Insertion of Ca²⁺ into XoxF1 had been an open question because low MDH activity was reported for enzyme purified from culture medium without added Ln³⁺ (59). In this study, we corroborate those results and provide evidence that WT XoxF1 coordinates an equimolar ratio of Ca²⁺ when Ln³⁺ are not available. The mxa operon encoding MxaFI also contains genes that code for accessory proteins involved in enzyme maturation and metal insertion (47). Genes encoding a cognate cytochrome c_L (xoxG) and an essential protein of unknown



function (xoxJ) are located in a cluster with xoxF1, but genes encoding a Ln³⁺ insertion system have yet to be identified (46). A separate gene cluster for lanthanide utilization and transport (lut), however, has been identified and characterized (66). The lut cluster contains several genes encoding Ln3+-binding proteins that also may facilitate metal insertion into XoxF1. WT XoxF1 possesses only La³⁺ when purified from culture medium containing both La³⁺ and Ca²⁺, indicating a selective preference for Ln³⁺. However, we observed high levels of Ca²⁺ in the D320A variant purified from the same culture conditions. These results suggest that Asp³²⁰ may be necessary not only for Ln³⁺ coordination at the active site, but also for Ln³⁺ selectivity. One possibility to explain this observation is that the supposed "metal-free" XoxF1 binds free Ca²⁺, which is available from the growth medium for transport to the periplasm. In any case, we propose that metal selection involves the active site residues with the participation of Asp³²⁰. We also observed high Ca²⁺ content in WT enzyme and the D320A variant when purified from culture medium without added La³⁺. Under this condition, the Ln switch cannot occur, and the *mxa* operon is expressed, including the genes encoding Ca2+ insertion proteins (21). It is possible that the Ca²⁺ insertion machinery encoded by the mxa cluster also recognizes XoxF1; however, additional components are not necessary for Ca2+ coordination by XoxF1. More detailed knowledge of the insertion machineries is needed to fully understand how Ln³⁺ are preferentially loaded into XoxF MDH and what distinguishes Ln³⁺ insertion from Ca2+ insertion. XoxF1 exhibits a clear preference for Ln3+, as corroborated by the inactivity of XoxF1 loaded with Ca²⁺ compared with that coordinating Ln³⁺. The Ca²⁺-bound XoxF1 exhibits low MDH activity using the dyelinked assay, even though high levels of the metal are present. Thus, XoxF1 from M. extorquens AM1 serves as a useful representative enzyme for comparing the impacts of Ln³⁺ versus Ca²⁺ on enzyme function because it can coordinate both metals. Kinetic, mutational, crystallographic, and DFT studies with the newly available XoxF1 structure (PDB entry 6OC6) will provide additional insight into how these metals affect XoxF MDH activity.

In addition to its Ln³⁺-dependent catalytic function, XoxF1 plays a role in regulation of the *mxa* and *xox1* operons. A copy of xoxF is required for mxa expression, leading to a proposed model where metal-free XoxF1 senses Ln3+ (43, 58). A xoxF suppressor mutant from the closely related *M. extorquens* PA1 is responsive to Ln3+, however, calling into question the essentiality of XoxF1 for Ln³⁺ sensing (67). It is worth noting that the suppressor mutations are located in the mxbD sensor kinase gene, whose product sits downstream of XoxF1 in the regulatory model. The resulting change to the HAMP domain of MxbD could affect signal transduction and obviate the need for XoxF1. Whereas there is debate regarding specific details of the complex regulatory cascade, it is the structure of XoxF—not the in vivo MDH catalytic activity—that is crucial for regulation. In this study, we provide further evidence supporting this model using catalytically nonfunctional XoxF1 D320A, which allows for growth with methanol in the absence of Ln³⁺. When either XoxF1 or the D320A variant is produced without Ln³⁺, the cultures grow similarly to the WT strain, suggesting that mxa

expression is similar to that in the WT cells. Using this condition, MxaFI catalyzes methanol oxidation, because XoxF1 does not bind ${\rm Ln^{3+}}$ and is inactive, as confirmed by our MDH assay results with pure enzymes. Our metal content analyses indicate that under these conditions, XoxF1 coordinates ${\rm Ca^{2+}}$. In addition, we observed ${\rm Ln^{3+}}$ -dependent growth phenotypes when producing XoxF1 D320A in the $\Delta xoxF1$ $\Delta xoxF2$ double mutant, indicating that ${\rm Ln^{3+}}$ were "sensed". This strain does not produce a functional XoxF1 capable of coordinating ${\rm Ln^{3+}}$, reaffirming the role of the XoxF protein in regulation rather than its catalytic activity. These results suggest that XoxF1 with ${\rm Ca^{2+}}$ may be an important signal for inducing MxaF1 production and further explain the binary metal loading preferences we observed by ICP-MS/OES analyses with purified enzymes.

In conclusion, our results have increased our understanding of ${\rm Ln}^{3+}$ ADH structure and function and provide two new crystal structures of XoxF1 MDH to the scientific community. These structures will aid in future endeavors to investigate ${\rm Ln}^{3+}$ and PQQ biochemistry.

Experimental procedures

Generation of MDH expression constructs

All strains and plasmids used in this study are listed in Table 1. XoxF1 was produced for crystallization screens using pNG284 (containing the P_{xox1} promoter, xoxF1 (META1_1740), and sequences encoding recombinant tobacco etch virus (TEV) protease cleavage site (68, 69) and a hexahistidine tag) in the WT strain of M. extorquens AM1 (21). To generate additional expression plasmids for enzyme production and complementation studies, PCR primers were designed with 20-40-bp overlaps between the plasmid backbone and gene inserts. For xoxF1 expression, pNG308 was constructed by replacing the P_{xox1} promoter in pNG284 with the M_{tac} promoter and ${
m RBS}_{fae}$ (70). We used pHC61 as the DNA template for the promoter with the RBS_{fae} sequence included in the forward primer. M_{tac} is constitutive in M. extorquens AM1. For exaF expression, pNG305 was generated using pNG308 as the DNA template for the backbone and pNG265 as the template for the exaF insert. The empty plasmid control, pNG311, was generated by linearizing pNG305 via PCR using a forward and reverse primer targeting the recombinant TEV cleavage site and RBS_{fae} respectively. Each primer was designed with an additional 20 bp of homology to its primer partner, allowing for recircularization of the now empty plasmid. All plasmids were assembled by gap repair assembly as described (21, 71). Amino acid substitutions were made using the Q5 site-directed mutagenesis kit (New England Biolabs, Ipswich, MA, USA) to generate pNG309 and pNG307 for expression of xoxF1 D320A and exaF D319S, respectively. All plasmids were verified by Sanger sequencing (Genewiz, South Plainfield, NJ, USA) and transformed into M. extorquens AM1 by triparental mating (21) or electroporation (72). Primers used for construct generation and mutagenesis are listed in Table S2.

Enzyme expression and purification

All glassware used for protein production cultures was precleaned of Ln by using it to grow the $\Delta mxaF$ strain on MP minimal medium (73) with 0.5% methanol. Cultures were grown with shaking at 200 rpm at 30 °C on an Innova 2300



platform shaker (Eppendorf, Hamburg, Germany) to maximal culture density. Flasks were cleaned and autoclaved, and this process was repeated until the $\Delta mxaF$ strain no longer grew above the initial optical density at 600 nm (OD_{600}), as described (21). For enzyme or variant protein enrichment, we scaled up to a 1.5-liter culture volume using 2.8-liter shake flasks and grew until reaching densities of OD₆₀₀ 1.5-6. Single colonies of strains were inoculated into 2 ml of minimal medium containing 2% succinate and 50 μg/ml kanamycin in 14-ml polypropylene culture tubes (Thermo Fisher Scientific, Waltham, MA, USA) and then grown to mid-exponential growth phase with shaking at 200 rpm and 30 °C on an Innova 2300 platform shaker. Large-scale cultures producing XoxF1 and XoxF1 D320A were grown with 0.5% methanol and 2 μ M LaCl₃ or 20 μΜ LaCl₃ for XoxF1 crystallization. Cells were harvested by centrifugation using a Sorvall RC6+ centrifuge (Thermo Fisher Scientific) at 21,000 \times g at 4 °C for 10 min. Extracts were prepared as described using an OS Cell Disrupter set at 25,000 p.s.i. (Constant Systems Ltd., Low March, Daventry, Northants, UK) (16). IMAC was used to purify enzymes as described (16). Enzyme enrichments were validated by SDS-PAGE analyses and desalted by buffer exchange into 25 mm Tris-HCl, 150 mm NaCl, pH 8.0, before measuring MDH activity.

Protein crystallization

The Ln-PQQ – bound protein crystals were obtained by mixing 0.65 μ l of ~2.5 mg/ml XoxF1 (reconstituted with equimolar La^{3+}) and 0.65 μ l of reservoir solution. The sitting drop reservoir contained 50 µl of 0.2 M ammonium chloride and 20% PEG 3350. Thin needles were briefly cryoprotected in 25% glycerol and 75% reservoir solution prior to freezing in liquid nitrogen. For the Ln-only bound protein crystals, we mixed 0.65 µl of \sim 2.5 mg/ml XoxF1 (reconstituted with equimolar La³⁺) and 0.65 µl of reservoir solution. The sitting-drop reservoir contained 50 μ l of 10% propanol, 0.1 μ HEPES, pH 7.5, and 20% PEG 4000. A large plate-shaped crystal was frozen directly in liquid nitrogen.

Diffraction data collection, structure determination, and analysis

X-ray diffraction data were collected at the Advanced Photon Source LS-CAT beamline 21-ID-F. Data sets were processed with xds (74) and HKL2000 (75), with merging and scaling done using aimless (76). Phases were solved with Phenix Phaser (77) using MDH from M. fumariolicum SolV (4MAE) as the starting model. Model building and refinement were conducted in COOT (78) and Phenix (79). Statistics for the data sets are listed in Table S1. Structure figures were created with UCSF Chimera (80) or PyMOL (81).

Metal quantification

Enzyme samples were deconstructed in 14-ml polypropylene tubes by heating at 90 °C for 1 h in 20% nitric acid. These samples were clarified of debris by centrifugation at 21,000 \times g for 20 min at room temperature using a Sorvall Legend X1R centrifuge (Thermo Fisher Scientific). One ml of supernatant was diluted with MilliQ water to a volume of 12 ml in a new polypropylene tube. Two independent samples of each protein variant were deconstructed in hot nitric acid for metal determination by ICP-AES for Ca²⁺ and ICP-MS for La³⁺. ICP-AES was used for Ca determination because of lower background measurements compared with ICP-MS. For La3+ quantification, samples were sent to the Laboratory for Environmental Analysis (Center of Applied Isotope Studies, University of Georgia) for analysis by ICP-MS. Ca2+ quantification of enzymes was determined using a Varian 710-ES ICP-AES (Agilent, Santa Clara, CA, USA). ICP-AES resulted in lower background levels compared with ICP-MS for Ca2+. A MilliQ water blank and desalting buffer were analyzed as controls for background La³⁺ and Ca²⁺ contamination.

Methanol dehydrogenase activity assays

MDH activity was measured by following the PMS-mediated reduction of DCPIP ($\epsilon_{600} = 21 \text{ mm}^{-1} \text{ cm}^{-1}$) (16, 21, 82) as described (60). The following notations are included for the assay preparation and execution: DCPIP and PMS were prepared in amber 1.5-ml Eppendorf tubes and kept on ice. Enzyme (3-100 μ g) was incubated with 10 μ l of 250 mM methanol or water (for no substrate controls) for 2 min at 30 °C before initiating the assay by the addition of 180 μ l of the dye mixture, prepared immediately beforehand at room temperature (16, 21). Little to no endogenous methanol-independent reduction of DCPIP was observed when following these modifications. Heat-inactivated enzyme controls used protein that was denatured at 95 °C for 10 min before the assay.

Complementation in liquid culture

Single colonies of strains were inoculated into 2 ml of Ln-free MP minimal medium (73) with 2% succinate and grown in 14 ml of polypropylene culture tubes (Thermo Fisher Scientific) to mid-exponential growth phase with shaking at 200 rpm on an Innova 2300 platform shaker, at 30 °C. Cells were harvested by centrifugation at $1,000 \times g$ for 10 min at room temperature using a Sorvall Legend X1R centrifuge. Spent culture medium was removed, and cell pellets were gently resuspended in 1 ml of Ln-free MP to wash the cells. This process was repeated a second time, after which the cells were resuspended to an OD_{600} of 6 to generate starting inocula for growth studies. Growth phenotypes were compared using a BioTek EpochII microplate reader (BioTek, Winooski, VT, USA) (21). Briefly, 10 μl of inoculum was added to 640 µl of growth medium with 0.5% methanol or 0.2% ethanol, 50 μ g/ml kanamycin, with or without 2 μΜ LaCl₃. MP medium contains 20 μΜ CaCl₂. Cultures were shaken at 548 rpm at 30 °C, and the OD₆₀₀ was monitored at 15-min intervals for 48-96 h. OD_{600} measurements were fitted to an exponential model for microbial growth using CurveFitter (RRID:SCR_018461). Growth curves were reproducible for a minimum of 12-18 distinct biological replicates from 3-4 independent experiments. Growth rates were calculated using a minimum of 40 data points. Lines of best fit were determined by an exponential model with a semi-log plot of OD_{600} versus time. R^2 values for all lines of best fit were > 0.99 for methanol-grown cultures and 0.98 for ethanol-grown culture.



Data availability

The crystal structure data sets have been deposited to the Protein Data Bank (55) with the identifiers 6OC5 and 6OC6. All other data are contained within the article.

Acknowledgments—We thank both C. Suriano and A. Locke for their assistance in generating expression constructs and performing growth curves.

Author contributions—N. M. G. and N. C. M.-G. conceptualization; N. M. G. and M. F. data curation; N. M. G., M. F., J. H., R. P. H., and N. C. M.-G. formal analysis; N. M. G., J. H., R. P. H., and N. C. M.-G. supervision; N. M. G. and M. F. validation; N. M. G., M. F., and K. D. investigation; N. M. G. and M. F. visualization; N. M. G. and M. F. methodology; N. M. G. writing-original draft; N. M. G., M. F., K. D., J. H., R. P. H., and N. C. M.-G. writing-review and editing; M. F., J. H., R. P. H., and N. C. M.-G. funding acquisition; J. H., R. P. H., and N. C. M.-G. project administration.

Funding and additional information—This material is based upon work supported by the National Science Foundation under Grants 1750003 (to N. C. M.-G. and N. M. G.) and CHE-1516126 (to R. P. H. and J. H.). M. F. was supported by University of Otago Health Sciences Postdoctoral Fellowship HSCDPD1703.

Conflict of interest—The authors declare that they have no conflicts of interest with the contents of this article.

Abbreviations—The abbreviations used are: PQQ, pyrroloquinoline quinone; DFT, density functional theory; MDH, methanol dehydrogenase; EDH, ethanol dehydrogenase; ADH, alcohol dehydrogenase; Ln-ADH, Ln³+-dependent alcohol dehydrogenase; IMAC, immobilized metal affinity chromatography; RMSD, root mean square deviation; PDB, Protein Data Bank; ANOVA, analysis of variance; PMS, phenazine methosulfate; DCPIP, 2,6-dichlorophenol indophenol; ICP, inductively coupled plasma; OES, optical emission spectroscopy; OD, optical density; RMSE, root mean square error; TEV, tobacco etch virus.

References

- Anthony, C. (2001) Pyrroloquinoline quinone (PQQ) and quinoprotein enzymes. Antioxid. Redox Signal. 3, 757–774 CrossRef Medline
- Anthony, C., and Ghosh, M. (1998) The structure and function of the PQQ-containing quinoprotein dehydrogenases. *Prog. Biophys. Mol. Biol.* 69, 1–21 CrossRef Medline
- Matsushita, K., Toyama, H., Yamada, M., and Adachi, O. (2002) Quinoproteins: structure, function, and biotechnological applications. *Appl. Mi*crobiol. Biotechnol. 58, 13–22 CrossRef Medline
- Choi, O., Kim, J., Kim, J.-G., Jeong, Y., Moon, J. S., Park, C. S., and Hwang, I. (2008) Pyrroloquinoline quinone is a plant growth promotion factor produced by *Pseudomonas fluorescens* B16. *Plant Physiol.* 146, 657–668 CrossRef Medline
- Killgore, J., Smidt, C., Duich, L., Romero-Chapman, N., Tinker, D., Reiser, K., Melko, M., Hyde, D., and Rucker, R. B. (1989) Nutritional importance of pyrroloquinoline quinone. *Science* 245, 850 – 852 CrossRef Medline
- Matsumura, H., Umezawa, K., Takeda, K., Sugimoto, N., Ishida, T., Samejima, M., Ohno, H., Yoshida, M., Igarashi, K., and Nakamura, N. (2014) Discovery of a eukaryotic pyrroloquinoline quinone-dependent oxidoreductase belonging to a new Auxiliary Activity family in the database of carbohydrate-active enzymes. *PLoS ONE* 9, e104851 CrossRef Medline
- 7. Takeda, K., Matsumura, H., Ishida, T., Samejima, M., Ohno, H., Yoshida, M., Igarashi, K., and Nakamura, N. (2015) Characterization of a novel

- PQQ-dependent quinohemoprotein pyranose dehydrogenase from *Co-prinopsis cinerea* classified into Auxiliary Activities family 12 in carbohydrate-active enzymes. *PLoS ONE* **10**, e0115722 CrossRef Medline
- 8. Sakuraba, H., Yokono, K., Yoneda, K., Watanabe, A., Asada, Y., Satomura, T., Yabutani, T., Motonaka, J., and Ohshima, T. (2010) Catalytic properties and crystal structure of quinoprotein aldose sugar dehydrogenase from hyperthermophilic archaeon *Pyrobaculum aerophilum*. *Arch. Biochem. Biophys.* **502**, 81–88 CrossRef Medline
- Anthony, C. (1982) The Biochemistry of Methylotrophs, Academic Press, Inc., New York
- Chistoserdova, L., and Lidstrom, M. (2013) Aerobic methylotrophic prokaryotes. in *The Prokaryotes*, 4th Ed. (Rosenberg, E., DeLong, E. F., Thompson, F., Lory, S., and Stackebrandt, E., eds) pp. 267–285, Springer, Berlin
- Chistoserdova, L., Kalyuzhnaya, M. G., and Lidstrom, M. E. (2009) The expanding world of methylotrophic metabolism. *Annu. Rev. Microbiol.* 63, 477–499 CrossRef Medline
- 12. Chistoserdova, L., and Kalyuzhnaya, M. G. (2018) Current trends in methylotrophy. *Trends Microbiol.* **26**, 703–714 CrossRef Medline
- 13. Skovran, E., and Martinez-Gomez, N. C. (2015) Just add lanthanides. *Science* **348**, 862–863 CrossRef Medline
- 14. Nakagawa, T., Mitsui, R., Tani, A., Sasa, K., Tashiro, S., Iwama, T., Hayakawa, T., and Kawai, K. (2012) A catalytic role of XoxF1 as La³⁺-dependent methanol dehydrogenase in *Methylobacterium extorquens* strain AM1. *PLoS ONE* 7, e50480 CrossRef Medline
- Pol, A., Barends, T. R. M., Dietl, A., Khadem, A. F., Eygensteyn, J., Jetten, M. S. M., and Op den Camp, H. J. M. (2014) Rare earth metals are essential for methanotrophic life in volcanic mudpots. *Environ. Microbiol.* 16, 255–264 CrossRef Medline
- Good, N. M., Vu, H. N., Suriano, C. J., Subuyuj, G. A., Skovran, E., and Martinez-Gomez, N. C. (2016) Pyrroloquinoline quinone-containing ethanol dehydrogenase in *Methylobacterium extorquens* AM1 extends lanthanide-dependent metabolism to multi-carbon substrates. *J. Bacteriol.* 198, 3109 –3118 CrossRef Medline
- Deng, Y. W., Ro, S. Y., and Rosenzweig, A. C. (2018) Structure and function of the lanthanide-dependent methanol dehydrogenase XoxF from the methanotroph *Methylomicrobium buryatense* 5GB1C. *J. Biol. Inorg. Chem.* 23, 1037–1047 CrossRef Medline
- 18. Chistoserdova, L. (2016) Lanthanides: New life metals? World J. Microbiol. Biotechnol. 32, 138 CrossRef Medline
- Hibi, Y., Asai, K., Arafuka, H., Hamajima, M., Iwama, T., and Kawai, K. (2011) Molecular structure of La³⁺-induced methanol dehydrogenase-like protein in *Methylobacterium radiotolerans*. *J. Biosci. Bioeng.* 111, 547–549 CrossRef Medline
- Daumann, L. J. (2019) Essential and ubiquitous: the emergence of lanthanide metallobiochemistry. *Angew. Chem. Int. Ed. Engl.* 58, 12795–12802 CrossRef Medline
- Good, N. M., Moore, R. S., Suriano, C. J., and Martinez-Gomez, N. C. (2019) Contrasting in vitro and in vivo methanol oxidation activities of lanthanide-dependent alcohol dehydrogenases XoxF1 and ExaF from Methylobacterium extorquens AM1. Sci. Rep. 9, 4248 CrossRef Medline
- Huang, J., Yu, Z., and Chistoserdova, L. (2018) Lanthanide-dependent methanol dehydrogenases of XoxF4 and XoxF5 clades are differentially distributed among methylotrophic bacteria and they reveal different biochemical properties. Front. Microbiol. 9, 1366 CrossRef Medline
- Wang, L., Suganuma, S., Hibino, A., Mitsui, R., Tani, A., Matsumoto, T., Ebihara, A., Fitriyanto, N. A., Pertiwiningrum, A., Shimada, M., Hayakawa, T., and Nakagawa, T. (2019) Lanthanide-dependent methanol dehydrogenase from the legume symbiotic nitrogen-fixing bacterium *Bradyrhizobium diazoefficiens* strain USDA110. *Enzyme Microb. Technol.* 130, 109371 CrossRef Medline
- Wu, M. L., Wessels, J. C., Pol, A., Op den Camp, H. J. M., Jetten, M. S. M., and van Niftrik, L. (2015) XoxF-type methanol dehydrogenase from the anaerobic methanotroph "Candidatus Methylomirabilis oxyfera". Appl. Environ. Microbiol. 81, 1442–1451 CrossRef Medline
- 25. Green, P. N., and Ardley, J. K. (2018) Review of the genus *Methylobacte-rium* and closely related organisms: a proposal that some *Methylobacte-*



- rium species be reclassified into a new genus, Methylorubrum gen. nov. Int. J. Syst. Evol. Microbiol. 68, 2727-2748 CrossRef Medline
- 26. Huang, J., Yu, Z., Groom, J., Cheng, J.-F. F., Tarver, A., Yoshikuni, Y., and Chistoserdova, L. (2019) Rare earth element alcohol dehydrogenases widely occur among globally distributed, numerically abundant and environmentally important microbes. ISME J. 13, 2005-2017 CrossRef Medline
- 27. Wegner, C. E., Gorniak, L., Riedel, S., Westermann, M., and Küsel, K. (2019) Lanthanide-dependent methylotrophs of the family Beijerinckiaceae: physiological and genomic insights. Appl. Environ. Microbiol. 86, e01830-19 CrossRef Medline
- 28. Keltjens, J. T., Pol, A., Reimann, J., and Op den Camp, H. J. M. (2014) PQQ-dependent methanol dehydrogenases: rare-earth elements make a difference. Appl. Microbiol. Biotechnol. 98, 6163-6183 CrossRef Medline
- 29. Wehrmann, M., Billard, P., Martin-Meriadec, A., Zegeye, A., and Klebensberger, J. (2017) Functional role of lanthanides in enzymatic activity and transcriptional regulation of pyrroloquinoline quinone-dependent alcohol dehydrogenases in Pseudomonas putida KT2440. mBio 8, e00570-17 CrossRef Medline
- 30. Vorholt, J. A. (2012) Microbial life in the phyllosphere. Nat. Rev. Microbiol. 10, 828 - 840 CrossRef Medline
- 31. Chistoserdova, L. (2019) New pieces to the lanthanide puzzle. Mol. Microbiol. 111, 1127-1131 CrossRef Medline
- 32. Chistoserdova, L. (2011) Methylotrophy in a lake: from metagenomics to single-organism physiology. Appl. Environ. Microbiol. 77, 4705-4711 CrossRef Medline
- 33. Taubert, M., Grob, C., Howat, A. M., Burns, O. J., Dixon, J. L., Chen, Y., and Murrell, J. C. (2015) XoxF encoding an alternative methanol dehydrogenase is widespread in coastal marine environments. Environ. Microbiol. 17, 3937-3948 CrossRef Medline
- 34. Richardson, I. W., and Anthony, C. (1992) Characterization of mutant forms of the quinoprotein methanol dehydrogenase lacking an essential calcium ion. Biochem. J. 287, 709-715 CrossRef Medline
- 35. Görisch, H., and Rupp, M. (1989) Quinoprotein ethanol dehydrogenase from Pseudomonas. Antonie Van Leeuwenhoek 56, 35-45 CrossRef Medline
- 36. Oubrie, A., Rozeboom, H. J., Kalk, K. H., Huizinga, E. G., and Dijkstra, B. W. (2002) Crystal structure of quinohemoprotein alcohol dehydrogenase from Comamonas testosteroni: structural basis for substrate oxidation and electron transfer. J. Biol. Chem. 277, 3727-3732 CrossRef Medline
- 37. Anthony, C. (1996) Quinoprotein-catalysed reactions. Biochem. J. 320, 697–711 CrossRef Medline
- 38. Ghosh, M., Anthony, C., Harlos, K., Goodwin, M. G., and Blake, C. (1995) The refined structure of the quinoprotein methanol dehydrogenase from Methylobacterium extorquens at 1.94 Å. Structure 3, 177-187 CrossRef Medline
- 39. Diehl, A., von Wintzingerode, F., and Görisch, H. (1998) Quinoprotein ethanol dehydrogenase of Pseudomonas aeruginosa is a homodimer: sequence of the gene and deduced structural properties of the enzyme. Eur. J. Biochem. 257, 409-419 CrossRef Medline
- 40. Lumpe, H., Pol, A., Op den Camp, H. J. M., and Daumann, L. J. (2018) Impact of the lanthanide contraction on the activity of a lanthanide-dependent methanol dehydrogenase: a kinetic and DFT study. Dalton Trans. 47, 10463-10472 CrossRef Medline
- 41. Bogart, J. A., Lewis, A. J., and Schelter, E. J. (2015) DFT study of the active site of the XoxF-type natural, cerium-dependent methanol dehydrogenase enzyme. Chemistry 21, 1743-1748 CrossRef Medline
- 42. Prejanò, M., Marino, T., and Russo, N. (2017) How can methanol dehydrogenase from Methylacidiphilum fumariolicum work with the alien Ce III ion in the active center? A theoretical study. Chemistry 23, 8652-8657 CrossRef Medline
- 43. Vu, H. N., Subuyuj, G. A., Vijayakumar, S., Good, N. M., Martinez-Gomez, N. C., and Skovran, E. (2016) Lanthanide-dependent regulation of methanol oxidation systems in Methylobacterium extorquens AM1 and their contribution to methanol growth. J. Bacteriol. 198, 1250-1259 CrossRef Medline

- 44. Skovran, E., Raghuraman, C., and Martinez-Gomez, N. C. (2019) Lanthanides in methylotrophy. in Methylotrophs and Methylotroph Communities (Chistoserdova, L., ed) pp. 101-116, Caister Academic Press, Seattle, WA
- 45. Martinez-Gomez, N. C., Vu, H. N., and Skovran, E. (2016) Lanthanide chemistry: from coordination in chemical complexes shaping our technology to coordination in enzymes shaping bacterial metabolism. Inorg. Chem. 55, 10083-10089 CrossRef Medline
- Vuilleumier, S., Chistoserdova, L., Lee, M.-C., Bringel, F., Lajus, A., Zhou, Y., Gourion, B., Barbe, V., Chang, J., Cruveiller, S., Dossat, C., Gillett, W., Gruffaz, C., Haugen, E., Hourcade, E., et al. (2009) Methylobacterium genome sequences: a reference blueprint to investigate microbial metabolism of C1 compounds from natural and industrial sources. PLoS ONE 4, e5584 CrossRef Medline
- 47. Chistoserdova, L. V., and Lidstrom, M. E. (1996) Molecular characterization of a chromosomal region involved in the oxidation of acetyl-CoA to glyoxylate in the isocitrate-lyase-negative methylotroph Methylobacterium extorquens AM1. Microbiology 142, 1459 – 1468 CrossRef Medline
- 48. Farhan Ul Haque, M., Kalidass, B., Bandow, N., Turpin, E. A., DiSpirito, A. A., and Semrau, J. D. (2015) Cerium regulates expression of alternative methanol dehydrogenases in Methylosinus trichosporium OB3b. Appl. Environ. Microbiol. 81, 7546-7552 CrossRef Medline
- Jahn, B., Pol, A., Lumpe, H., Barends, T., Dietl, A., Hogendoorn, C., Op den Camp, H., and Daumann, L. (2018) Similar but not the same: first kinetic and structural analyses of a methanol dehydrogenase containing a europium ion in the active site. Chembiochem CrossRef Medline
- 50. Xia, Z. X., Dai, W. W., Xiong, J. P., Hao, Z. P., Davidson, V. L., White, S., and Mathews, F. S. (1992) The three-dimensional structures of methanol dehydrogenase from two methylotrophic bacteria at 2.6-Å resolution. J. Biol. Chem. 267, 22289 – 22297 Medline
- 51. Culpepper, M. A., and Rosenzweig, A. C. (2014) Structure and proteinprotein interactions of methanol dehydrogenase from Methylococcus capsulatus (Bath). Biochemistry 53, 6211-6219 CrossRef Medline
- 52. Cao, T. P., Choi, J. M., Kim, S. W., and Lee, S. H. (2018) The crystal structure of methanol dehydrogenase, a quinoprotein from the marine methylotrophic bacterium Methylophaga aminisulfidivorans MPT. J. Microbiol. 56, 246-254 CrossRef Medline
- 53. Anthony, C., and Williams, P. (2003) The structure and mechanism of methanol dehydrogenase. Biochim. Biophys. Acta 1647, 18-23 CrossRef
- 54. El-Gebali, S., Mistry, J., Bateman, A., Eddy, S. R., Luciani, A., Potter, S. C., Qureshi, M., Richardson, L. J., Salazar, G. A., Smart, A., Sonnhammer, E. L. L., Hirsh, L., Paladin, L., Piovesan, D., Tosatto, S. C. E., and Finn, R. D. (2019) The Pfam protein families database in 2019. Nucleic Acids Res. 47, D427-D432 CrossRef Medline
- 55. Berman, H. M., Battistuz, T., Bhat, T. N., Bluhm, W. F., Bourne, P. E., Burkhardt, K., Feng, Z., Gilliland, G. L., Iype, L., Jain, S., Fagan, P., Marvin, J., Padilla, D., Ravichandran, V., Schneider, B., et al. (2002) The Protein Data Bank. Acta Crystallogr. D Biol. Crystallogr. 58, 899-907 CrossRef
- 56. Holm, L. (2019) Benchmarking fold detection by DaliLite v.5. Bioinformatics 35, 5326-5327 CrossRef Medline
- 57. Tsushima, S. (2019) Lanthanide-induced conformational change of methanol dehydrogenase involving coordination change of cofactor pyrroloquinoline quinone. Phys. Chem. Chem. Phys. 21, 21979 -21983 CrossRef Medline
- 58. Skovran, E., Palmer, A. D., Rountree, A. M., Good, N. M., and Lidstrom, M. E. (2011) XoxF is required for expression of methanol dehydrogenase in Methylobacterium extorquens AM1. J. Bacteriol. 193, 6032-6038 CrossRef Medline
- Schmidt, S., Christen, P., Kiefer, P., and Vorholt, J. A. (2010) Functional investigation of methanol dehydrogenase-like protein XoxF in Methylobacterium extorquens AM1. Microbiology 156, 2575-2586 CrossRef Medline
- 60. Anthony, C., and Zatman, L. J. (1967) The microbial oxidation of methanol. The prosthetic group of the alcohol dehydrogenase of Pseudomonas sp. M27: a new oxidoreductase prosthetic group. Biochem. J. 104, 960-969 CrossRef Medline



- Görisch, H. (2003) The ethanol oxidation system and its regulation in Pseudomonas aeruginosa. Biochim. Biophys. Acta 1647, 98 – 102 CrossRef Medline
- Mutzel, A., and Görisch, H. (1991) Quinoprotein ethanol dehydrogenase: preparation of the apo-form and reconstitution with pyrroloquinoline quinone and Ca or Sr ions. *Agric. Biol. Chem.* 55, 1721–1726 CrossRef
- Rupp, M., and Görisch, H. (1988) Purification, crystallisation and characterization of quinoprotein ethanol dehydrogenase from *Pseudomonas aeruginosa*. *Biol. Chem. Hoppe Seyler* 369, 431–439 CrossRef Medline
- 64. Toyama, H., Mathews, F. S., Adachi, O., and Matsushita, K. (2004) Quinohemoprotein alcohol dehydrogenases: structure, function, and physiology. *Arch. Biochem. Biophys.* **428**, 10–21 CrossRef Medline
- 65. Featherston, E. R., Rose, H. R., McBride, M. J., Taylor, E. M., Boal, A. K., and Cotruvo, J. A. (2019) Biochemical and structural characterization of XoxG and XoxJ and their roles in lanthanide-dependent methanol dehydrogenase activity. *Chembiochem* 20, 2360 –2372 CrossRef Medline
- 66. Roszczenko-Jasińska, P., Vu, H. N., Subuyuj, G. A., Crisostomo, R. V., Cai, J., Raghuraman, C., Ayala, E. M., Clippard, E. J., Lien, N. F., Ngo, R. T., Yarza, F., Hoeber, C. A., Martinez-Gomez, N. C., and Skovran, E. (2019) Lanthanide transport, storage, and beyond: genes and processes contributing to XoxF function in *Methylorubrum extorquens* AM1. *bioRxiv* CrossRef
- Ochsner, A. M., Hemmerle, L., Vonderach, T., Nüssli, R., Bortfeld-Miller, M., Hattendorf, B., and Vorholt, J. A. (2019) Use of rare-earth elements in the phyllosphere colonizer *Methylobacterium extorquens* PA1. *Mol. Microbiol.* 111, 1152–1166 CrossRef Medline
- 68. Stols, L., Gu, M., Dieckman, L., Raffen, R., Collart, F. R., and Donnelly, M. I. (2002) A new vector for high-throughput, ligation-independent cloning encoding a tobacco etch virus protease cleavage site. *Protein Expr. Purif.* 25, 8–15 CrossRef Medline
- Blommel, P. G., and Fox, B. G. (2007) A combined approach to improving large-scale production of tobacco etch virus protease. *Protein Expr. Purif.* 55, 53–68 CrossRef Medline
- 70. Chou, H.-H., Berthet, J., and Marx, C. J. (2009) Fast growth increases the selective advantage of a mutation arising recurrently during evolution under metal limitation. *PLoS Genet.* **5**, e1000652 CrossRef Medline
- Jacobus, A. P., and Gross, J. (2015) Optimal cloning of PCR fragments by homologous recombination in *Escherichia coli. PLoS ONE* 10, e0119221 CrossRef Medline
- Toyama, H., Anthony, C., and Lidstrom, M. E. (1998) Construction of insertion and deletion mxa mutants of Methylobacterium extorquens AM1 by electroporation. FEMS Microbiol. Lett. 166, 1–7 CrossRef Medline
- 73. Delaney, N. F., Kaczmarek, M. E., Ward, L. M., Swanson, P. K., Lee, M.-C., and Marx, C. J. (2013) Development of an optimized medium, strain and high-throughput culturing methods for *Methylobacterium extorquens*. *PLoS ONE* 8, e62957 CrossRef Medline
- Kabsch, W. (2010) XDS. Acta Crystallogr. D Biol. Crystallogr. 66, 125–132 CrossRef Medline

- Otwinowski, Z., and Minor, W. (1997) Processing of X-ray diffraction data collected in oscillation mode. *Methods Enzymol.* 276, 307–326 CrossRef Medline
- Winn, M. D., Ballard, C. C., Cowtan, K. D., Dodson, E. J., Emsley, P., Evans, P. R., Keegan, R. M., Krissinel, E. B., Leslie, A. G. W., McCoy, A., McNicholas, S. J., Murshudov, G. N., Pannu, N. S., Potterton, E. A., Powell, H. R., et al. (2011) Overview of the CCP4 suite and current developments. Acta Crystallogr. D Biol. Crystallogr. 67, 235–242 CrossRef Medline
- McCoy, A. J., Grosse-Kunstleve, R. W., Adams, P. D., Winn, M. D., Storoni, L. C., and Read, R. J. (2007) Phaser crystallographic software. J. Appl. Crystallogr. 40, 658 674 CrossRef Medline
- Emsley, P., Lohkamp, B., Scott, W. G., and Cowtan, K. (2010) Features and development of Coot. Acta Crystallogr. D Biol. Crystallogr. 66, 486 –501 CrossRef Medline
- Afonine, P. V., Grosse-Kunstleve, R. W., Echols, N., Headd, J. J., Moriarty, N. W., Mustyakimov, M., Terwilliger, T. C., Urzhumtsev, A., Zwart, P. H., and Adams, P. D. (2012) Towards automated crystallographic structure refinement with phenix.refine. Acta Crystallogr. D Biol. Crystallogr. 68, 352–367 CrossRef Medline
- Pettersen, E. F., Goddard, T. D., Huang, C. C., Couch, G. S., Greenblatt, D. M., Meng, E. C., and Ferrin, T. E. (2004) UCSF Chimera: a visualization system for exploratory research and analysis. *J. Comput. Chem.* 25, 1605–1612 CrossRef Medline
- DeLano, W. L. (2012) The PyMOL Molecular Graphics System, version 1.5.0.1–2.2.3, Schroedinger, LLC, New York
- McArmstrong, J. M. (1964) The molar extinction coefficient of 2,6-dichlorophenol indophenol. *Biochim. Biophys. Acta* 86, 194–197 CrossRef Medline
- 83. Simon, R., Priefer, U., and Pühler, A. (1983) A broad host range mobilization system for *in vivo* genetic engineering: transposon mutagenesis in Gram negative bacteria. *Nat. Biotechnol.* 1, 784–791 CrossRef
- 84. Nunn, D. N., and Lidstrom, M. E. (1986) Isolation and complementation analysis of 10 methanol oxidation mutant classes and identification of the methanol dehydrogenase structural gene of *Methylobacterium* sp. strain AM1. *J. Bacteriol.* 166, 581–590 CrossRef Medline
- Marx, C. J., O'Brien, B. N., Breezee, J., and Lidstrom, M. E. (2003) Novel methylotrophy genes of *Methylobacterium extorquens* AM1 identified by using transposon mutagenesis including a putative dihydromethanopterin reductase. *J. Bacteriol.* 185, 669 – 673 CrossRef Medline
- 86. Figurski, D. H., and Helinski, D. R. (1979) Replication of an origin-containing derivative of plasmid RK2 dependent on a plasmid function provided in *trans. Proc. Natl. Acad. Sci. U.S.A.* **76**, 1648–1652 CrossRef
- 87. Williams, P. A., Coates, L., Mohammed, F., Gill, R., Erskine, P. T., Coker, A., Wood, S. P., Anthony, C., and Cooper, J. B. (2005) The atomic resolution structure of methanol dehydrogenase from *Methylobacterium extorquens*. *Acta Crystallogr. D Biol. Crystallogr.* **61**, 75–79 CrossRef Medline
- Keitel, T., Diehl, A., Knaute, T., Stezowski, J. J., Höhne, W., and Görisch, H.
 (2000) X-ray structure of the quinoprotein ethanol dehydrogenase from Pseudomonas aeruginosa: basis of substrate specificity. J. Mol. Biol. 297, 961–974 CrossRef Medline

